

# Ternary Alkali Metal Copper Chalcogenides ACuX (A= Na, K and X= S, Se, Te): Promising Candidate for Solar Harvesting Applications

Gurudayal Behera,<sup>1</sup> Surabhi Suresh Nair,<sup>2</sup> Nirpendra Singh,<sup>2</sup> K. R. Balasubramaniam,<sup>1,\*</sup> and Aftab Alam<sup>3,†</sup>

<sup>1</sup>*Department of Energy Science and Engineering, IIT Bombay, Powai, Mumbai 400076, India*

<sup>2</sup>*Department of Physics, Khalifa University of Science and Technology, Abu Dhabi 127788, United Arab Emirates*

<sup>3</sup>*Department of Physics, Indian Institute of Technology, Bombay, Powai, Mumbai 400076, India*

(Dated: December 27, 2023)

We report a comprehensive first-principles study of the relative stability of the various possible crystal structures, and the electronic and optical properties of ternary alkali metal chalcogenides ACuX (A= Na/K and X= S/Se/Te) compounds through density functional theory (DFT) calculations. The energetics and phonon spectra of greater than 700 structures were compared, and seven possible stabilized structures of six ACuX compounds were identified using the fixed composition evolutionary search method. Our electronic band structure simulation confirms that all the ternary ACuX compounds are direct band gap semiconductors, with the band gap lying between 0.83 eV to 2.88 eV. These compounds exhibit directly allowed electronic transitions from the valence band to the conduction band, which leads to a significant strength of optical transition probability. This yields a sharp rise in the optical absorption spectra (ranging between  $10^4$  to  $10^5$  cm<sup>-1</sup>) near the energy gap. The estimated spectroscopic limited maximum efficiency (SLME) is about 18% for an 8  $\mu$ m thick NaCuTe film. For other ACuX compounds, the SLME ranges between 10% to 13%. In addition, we also explored the feasibility of these ternary ACuX compounds for photocatalytic water splitting applications and found that they can be promising candidates as photocathodes for hydrogen evolution reactions. With a large spread in the band gap and interesting band topology near Fermi level, these chalcogenides can be quite fertile for other energy applications such as thermoelectric, LED, *etc.*

## I. INTRODUCTION

In recent years, multinary chalcogenide semiconductors have witnessed extensive applications in the development of thin-film solar photovoltaic (PV) devices. For example, CuIn<sub>1-x</sub>(Se,Te)<sub>2</sub> (CIGS), Cu<sub>2</sub>ZnSnS<sub>4</sub>, CdTe, SnS, Sb<sub>2</sub>S<sub>3</sub>, *etc.* have shown immense promise in thin film solar cells [1–4]. Among them, CdTe and CIGS are most prevalent due to their direct band gaps and high light absorption capabilities, enabling them to achieve notable solar cell efficiencies [5–8]. It is however also known that CdTe and CIGS come with certain drawbacks. They contain toxic elements, namely Cd and Te, as well as elements that are relatively scarce in the earth's crust, such as Te, In, and Ga, which is a major concern that could limit market feasibility for sustainable, cost-effective, and large-scale manufacturing. Thus, identifying efficient light absorber materials in thin film-based PV devices with band gaps in the visible range is a crucial challenge. Apart from this, there are few other major issues in existing solar absorbers employed in PV devices are *e.g.*, organic moieties that cause degradation over short carrier lifetimes (*i.e.*, organic/inorganic halide perovskites [8–11]), and the presence of defect states causing high recombination rate [12, 13]. As such, finding alternative materials is an urgent need of the hour. The material should acquire few prerequisite criteria such as low

cost (abundant), high carrier lifetime, high absorption and defect tolerance.

Recently, alkali metal ternary copper telluride ACuTe (A=Na, K) has been proposed to be efficient light absorber for thin film solar cells, satisfying most of the above criteria [14]. They are reported to be direct band gap semiconductors having band gap values of 1.43 eV and 1.63 eV for NaCuTe and KCuTe, respectively. The high absorption coefficient ( $\sim 10^4$  cm<sup>-1</sup>) in the visible range and a reasonably high carrier lifetime due to low deep level defects suggest their potentiality as efficient solar absorbers. The high abundance of constituent elements is an added advantage. This has motivated us to further investigate the feasibility of other chalcogenides (S and Se) based ternary compounds as solar absorbers.

The ternary alkali metal copper chalcogenides ACuX (A=Na, K and X=S, Se, Te) have been experimentally synthesized by Savelsberg and Schfer in 1978 [15, 16]. They found that KCuS crystallizes in orthorhombic structure (space group Pna2<sub>1</sub>), while KCuSe/Te has a hexagonal structure with space group P6<sub>3</sub>/mmc. Similarly, NaCuSe/Te is reported to crystallize in tetragonal structures with space group P4/nmm. Since then, no further experimental as well as theoretical studies have been reported on this class of compounds. Recently, Vaitheeswaran *et al.* [17] studied the structural, electronic, and optical properties of ternary KCuSe and KCuTe using *ab-initio* calculations. They reported these compounds to be semiconductors with suitable band gaps that could be promising as solar absorbers in PV, photodetectors, and other optoelectronic device applications. On a similar line, Boualleg *et al.* [18] reported the phase

\* bala.ramanathan@iitb.ac.in

† aftab@iitb.ac.in

transition and thermal properties of KCuSe and KCuTe. They reported these two compounds to stabilize in orthorhombic and tetragonal phases, respectively in contrast to the experimental hexagonal structure. The dynamical stability study also confirmed the existence of other possible crystal structures for KCuSe and KCuTe compounds. For other ternary chalcogenides *i.e.*, NaCuSe, NaCuTe, and KCuS, no further studies (both experiment and theory) are reported reassessing their crystal structures. NaCuS is never reported earlier and hence its crystal structure is not known. The conflict between experimental and theoretically predicted crystal structures and the prediction of the most stable structural phases needs to be addressed. In addition, a thorough study to investigate the potential of all these ternary compounds for various solar harnessing applications can be extremely useful.

In this work, we aim to present a detailed insight into the structural stability, electronic, and optical properties of ternary ACuX compounds assessing their potential as efficient light absorber using first-principles Density Functional Theory (DFT) calculations. In particular, we utilized a fixed composition evolutionary search method to accurately predict the correct crystal structure of all these six compounds. The method generates greater than 700 structures (depending on the system) and scrutinize the most stable out of them based on certain factors. This has been a powerful method to predict ground state structures for a given system. Interestingly, though the crystal structure of a few systems matches with those predicted experimentally, there are other systems where the most stable structure is few meV lower in energy as compared to the experimental ones. Lattice dynamics calculations are also performed in parallel to evaluate the dynamically stable structures for each compound. We further simulated the electronic and optical properties of all six ACuX (A=Na/K, X=S/Se/Te) compounds in their most stable phases. All six ACuX compounds are found to be direct band gap semiconductors with band gap values ranging between 0.83 eV to 2.88 eV. These band gaps are simulated using the most accurate hybrid exchange-correlation functional. The optical simulation confirms the anisotropic nature of the absorption spectra having different in-plane and out-of-plane values, with absorption coefficient  $\sim 10^4 \text{ cm}^{-1}$  in the visible range. The theoretically predicted spectroscopic limited maximum efficiency (SLME) is found to lie in the range 10 % to 18 % for a thickness of 8 to 10  $\mu\text{m}$  under 1 sun illumination AM1.5G. Further, we evaluated the potential of all stable ACuX compounds as photocathodes for water splitting applications based on their band edge positions with respect to water redox potential.

## II. COMPUTATIONAL DETAILS

The fixed composition evolutionary search method is utilized for predicting the crystal structure, as employed

in the USPEX package[19–21]. An initial population of 20 structures is generated randomly[20], while the subsequent generations are produced due to variation operators, which include heredity (50%), random symmetric structure generation (30%), and soft mutation (20%). Subsequently, a comprehensive exploration is carried out by generating more than 700 crystal structures depending on the six compounds. Our enthalpy calculations based on DFT identify optimal structures from each generation within the selection criterion. The procedure for local optimization is executed in a five-step process utilizing the generalized gradient approximation (GGA)[22] within the Perdew-Burke-Ernzerhof functional (PBE)[23], implemented in the Vienna Ab-initio Simulation Package (VASP) [24–26]. For a more accurate calculation of the electronic structure (band gap), the screened hybrid HSE06 functional [27, 28] was employed. The kinetic energy cut-off for the plane wave basis set was set to 520 eV. The Brillouin zone (BZ) integration was done using a  $\Gamma$ -centered scheme with  $12 \times 12 \times 6$  k-meshes for ionic relaxations and  $16 \times 16 \times 8$  for self-consistent-field calculations. The density of states (DOS) was calculated using the tetrahedron method with Blöch corrections[29]. Electronic band structure within the HSE06 was simulated using  $8 \times 8 \times 4$  k-mesh. All the atoms in the unit cell are fully relaxed using the conjugate gradient method until the force (energy) converges below 0.001 eV/Å ( $10^{-7}$  eV). The phonon spectra are calculated using the supercell approach as implemented in the phonopy package [30, 31]. Effect of spin-orbit coupling (SOC) was included for all the compounds. Formation energy ( $\Delta E_F$ ) of ACuX (A; Na/K and X; S/Se/Te) were calculated using the following expression,

$$\Delta E_F = \frac{E_{Tot} - [nE_A - lE_{Cu} - mE_X]}{N} \quad (1)$$

where “ $E_{Tot}$ ” is the total energy of the target compound, “ $n$ ”, “ $l$ ”, and “ $m$ ” are the numbers of Na/K, Cu, and S/Se/Te atoms present in the compound, while  $N$  is the total number of atoms present in the cell.  $E_A$ ,  $E_{Cu}$ , and  $E_X$  are the total energies per atom of the constituent elements in their respective bulk equilibrium structures.

To simulate the optical properties, the frequency-dependent dielectric constants were calculated within the independent particle approximation (IPA) [32–34], as implemented in VASP. To measure the theoretical maximum possible efficiency, we have used an improved version of the Shockley-Queisser (SQ) efficiency limit known as spectroscopic limited maximum efficiency (SLME) proposed by Yu *et al.* [35] using SL3ME code[36]. More details about the theoretical formulation of optical calculations and SLME can be found in Sec I of the supplementary information (SI)[37].

TABLE I. Formation energies ( $\Delta E_F$ ) of experimentally reported and theoretically simulated lowest energy structures for six ACuX compounds. ‘\*’ indicates the experimentally reported space groups.  $\Delta$  is the energy difference between the  $\Delta E_F$  of experimental and theoretical structures.

Compounds	Space Group	$\Delta E_F$ (meV/atom)	$\Delta$ (meV/atom)
NaCuS	Pna2 <sub>1</sub>	-708	Not synthesized
NaCuSe	P4/nmm*[15]	-617	20
	P6 <sub>3</sub> /mmc	-637	
NaCuTe	P4/nmm*[15]	-493	17
	P6 <sub>3</sub> /mmc	-510	
KCuS	Pna2 <sub>1</sub> *[16]	-768	
KCuSe	P6 <sub>3</sub> /mmc*	-687	12
	Pnma[15]	-695	
KCuTe	P6 <sub>3</sub> /mmc*[15]	-595	

### III. RESULTS AND DISCUSSION

#### A. Energetics and Dynamical Stability of ACuX

Out of all the structures (more than 700 structures) generated by USPEX package [19–21], we selected nine structures with the lowest formation energies for each ternary ACuX (A= Na, K and X=S, Se, and Te) compounds. The space groups (SG) of these nine structures are Pnma, Pna2<sub>1</sub>, P6<sub>3</sub>/mmc, P4/nmm, Cmc, P2<sub>1</sub>/m, F43m, P6<sub>3</sub>mc, and C2/c, respectively. The prototype crystal structures of such space groups are shown in Fig. S1 of the SI [37] and their optimized lattice parameters and corresponding formation energies obtained from DFT calculations for all the six different ACuX compounds are listed in Table S1 to S6 in SI [37]. Table I display the space group and formation energies ( $\Delta E_F$ ) of the experimentally reported crystal structures and the energetically most stable simulated crystal structures and their energy difference ( $\Delta$ ). It is observed from Table I that NaCuS (never studied before) crystallizes in the Pna2<sub>1</sub> space group. However, energetically NaCu(Se/Te) should stabilize in hexagonal structure (SG: P6<sub>3</sub>/mmc), whose  $\Delta E_F$  is  $\sim 17$ -20 meV/atom lower than those of experimentally reported tetragonal structure (space group P4/nmm). KCuS was found to stabilize in the orthorhombic structure having space groups Pna2<sub>1</sub>, which agrees with the experimental prediction[16]. In contrast, KCuSe is found to stabilize in the orthorhombic crystal structure, which is 12 meV/atom lower in energy than the experimentally reported hexagonal structure[15]. KCuTe stabilizes in the hexagonal structure (SG:P6<sub>3</sub>/mmc), which matches with the experimentally findings[15].

To further assess the phase stability, specially for NaCuSe, NaCuTe and KCuSe compounds where the experimental structure is higher in energy (by 12 to 20 meV/atom) as compared to the theoretically optimized one, we simulated their phonon dispersion which will help to evaluate the dynamical stability. The phonon dispersion for all the experimental and theoretically optimized ACuX compounds in different space groups (as shown in Table I) are shown in Fig. S2 of SI[37]. For NaCuS (SG: Pna2<sub>1</sub>), NaCuSe/Te (SG: P6<sub>3</sub>/mmc), and all the KCuX compounds in their respective space groups, the phonon frequencies are found to be positive, confirming the dynamical stability for all these compounds. A very small imaginary frequency appears at/around the  $\Gamma$  point in the orthorhombic structures of KCuSe (SG: Pnma), which may be due to the limited supercell size used in this calculation. Interestingly, the phonon spectrum for the experimentally reported NaCuSe and NaCuTe (SG: P4/nmm) show appreciable imaginary frequencies (see Fig. S2(b and d) of SI[37]), indicating their instability in tetragonal phase. Most likely, they crystallize in hexagonal crystal structure, *i.e.*, P6<sub>3</sub>/mmc space groups, which is favored by both formation energy and phonon dispersion data. We believe the structural characterization of these two systems should be revisited. In summary, based on the formation energies and phonon spectra, we have chosen seven most stable ternary ACuX compounds, *i.e.*, orthorhombic NaCuS and KCuS (SG: Pna2<sub>1</sub>), hexagonal NaCuSe/Te and KCuSe/Te (SG: P6<sub>3</sub>/mmc) and the orthorhombic & hexagonal KCuSe (SG: Pnma) to further explore their optoelectronic properties.

#### B. Electronic Structure

All the ternary ACuX compounds were theoretically optimized in their respective stable structures to calculate the electronic properties. The prototype crystal structures are shown in Fig 1, and the crystallographic parameters, such as lattice constants and bond lengths are tabulated in Table II. The optimized structural details are in fair agreement with the available experimental [15, 16] as well as theoretically [14, 17, 18] reported data. For ACuSe/Te which stabilizes in the hexagonal structure, Cu and Se/Te ions form honeycomb (hexagonal) layers along the c-direction, and between each hexagonal bilayer, there exists a triangular lattice of Na/K atoms (see Fig. 1(a)). The Na/K atoms are situated on top of the center of the honeycomb lattice, while Cu/Se/Te atoms are positioned on top of the center of the triangular lattice. In contrast, the lattice arrangement in orthorhombic structures for both the space groups (for Pna2<sub>1</sub> and Pnma) is slightly different, as shown in Fig 1(b and c). In both the cases, the X-Cu-X shows a linear chain with an angle of 180°.

The comparative band structure plots with and without spin-orbit coupling (SOC) within the PBE level are shown in Fig. S3 of SI[37]. As evident from Fig. S3, there

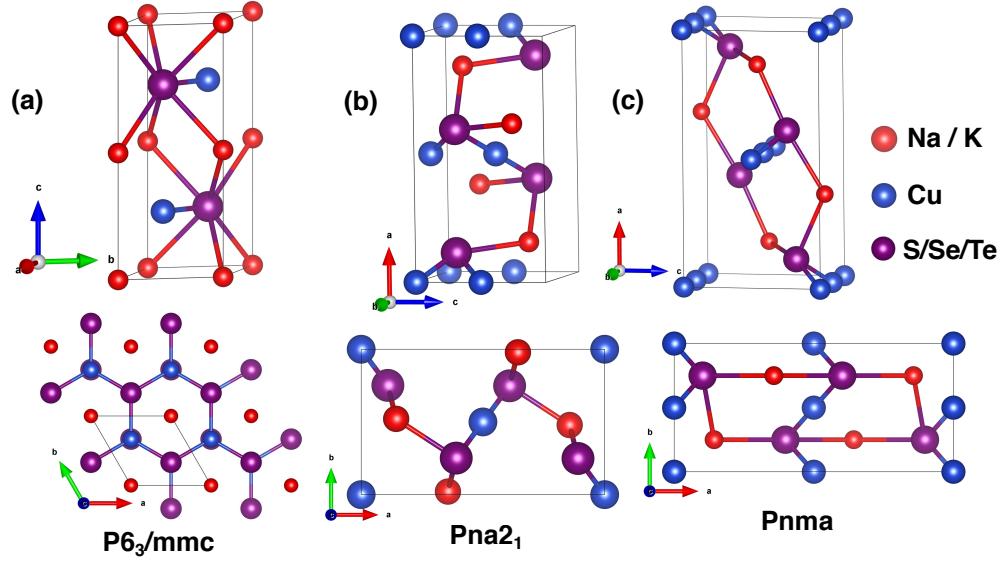


FIG. 1. Prototype crystal structures of ACuX compounds in different space groups, as reported in Table I (a) ACuX (X=Se, Te) ( $P6_3/mmc$ ), (b) ACuS ( $Pna2_1$ ), (c) KCuSe ( $Pnma$ ), respectively. The set of top and bottom figures indicate the view of the respective structures from (110) and (001) orientations, respectively.

TABLE II. Theoretically optimized lattice parameters, bond lengths, and band gaps of energetically most stable ACuX (A=Na, K; X=S, Se, Te) compounds. Experimental results[15, 16] are given wherever available.

Compounds	Space group	Lattice Constants (Å)	Bond length (Å)	Band gap (eV) PBE/HSE06
NaCuS	$Pna2_1$	$a = 9.48, b = 5.65$ $c = 5.13$	Cu-S = 2.17, Na-S = 2.89, 2.79	1.55/2.42
NaCuSe	$P6_3/mmc$	$a = 4.14, c = 8.34$	Cu-Se = 2.39, Na-Se = 3.17	0/0.83
NaCuTe	$P6_3/mmc$	$a = 4.42, c = 8.69$	Cu-Te = 2.55, Na-Te = 3.35	0.49/1.21
KCuS	$Pna2_1$	$a = 10.88, b = 6.34,$ $c = 5.34$ $a = 10.66, b = 6.20,$ $c = 5.32$ (exp.[16])	Cu-S = 2.16, K-S = 3.21, 3.19	1.88/2.88
KCuSe	$Pnma$	$a = 11.84, b = 5.43,$ $c = 6.36$	Cu-Se = 2.28, K-Se = 3.31, 3.39	1.72/2.67
	$P6_3/mmc$	$a = 4.20, c = 9.92$ $a = 4.18, c = 9.54$ (exp. [15])	Cu-Se = 2.43, K-Se = 3.47	0.11/1.28
KCuTe	$P6_3/mmc$	$a = 4.48, c = 10.31$ $a = 4.46, c = 9.95$ (exp.[14, 15])	Cu-Te = 2.59, K-Te = 3.65	0.52/1.62

is no change in band gap as well as band dispersion for S- and Se-based compounds. However, Te, a heavy element, slightly changes the band gap apart from the minor band splitting due to the SOC effect. For instance,  $E_g$  for NaCuTe changes from 0.49 eV (w/o SOC) to 0.36 eV (with SOC), and that for KCuTe changes from 0.52 eV (w/o SOC) to 0.41 eV (with SOC) in  $P6_3/mmc$  structure. Our PBE-SOC results for KCuSe and KCuTe corroborate well

with other theoretical reports[17]. As the SOC effect is not too significant, yet the band gap is conventionally underestimated within the PBE functional, we further performed the electronic structures of all the compounds using HSE06 functional without the SOC effect for more accurate band gap estimation.

Figure 2 shows the electronic band structures and the optical transition probability of all the ACuX com-

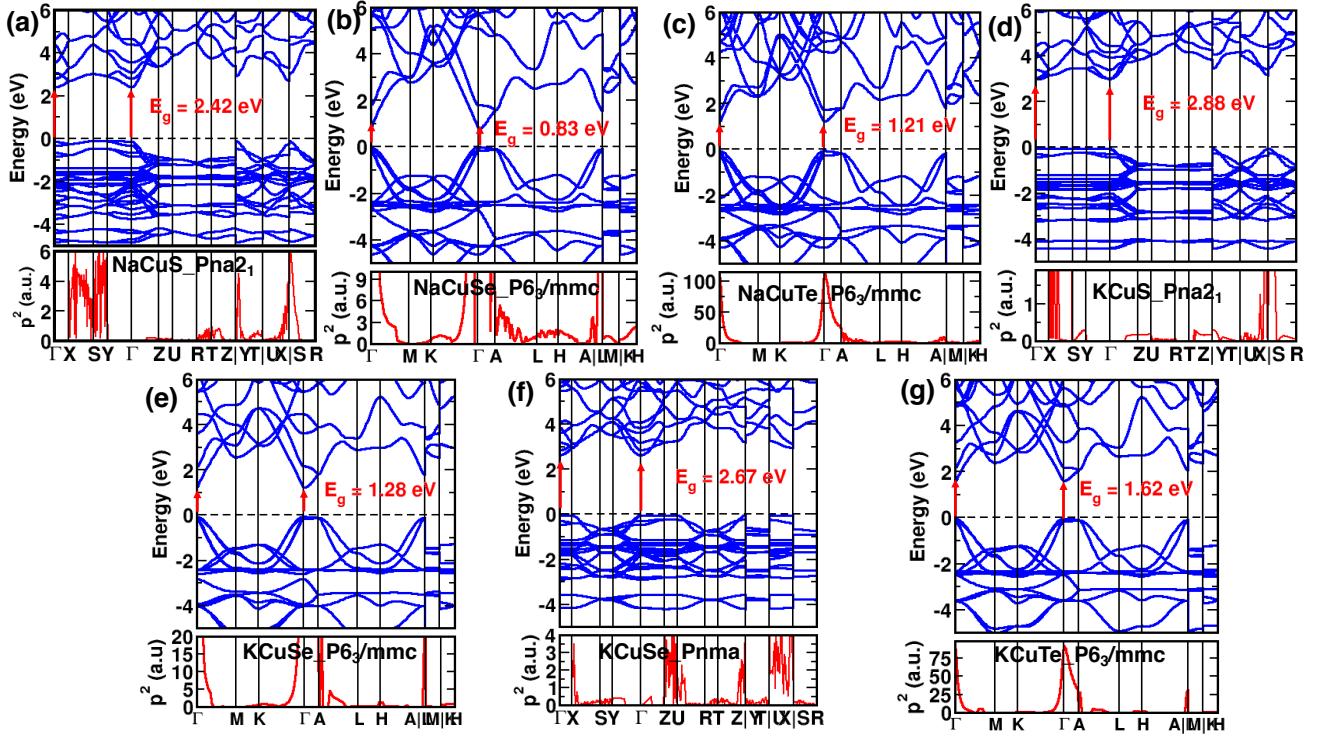


FIG. 2. Electronic band structures (above panels) and optical transition probabilities (square of dipole transition matrix elements) (below panels) of ACuX compounds in their respective lowest energy structure using HSE06 functional. For KCuSe, results for both  $P6_3/mmc$  and  $Pnma$  are shown due to a relatively small energy difference between the two. Fermi level ( $E_f$ ) is set at 0 eV.

pounds using hybrid (HSE06) functionals. All the compounds are direct band gap semiconductors in which the valance band maximum (VBM) and conduction band minimum (CBM) are located at  $\Gamma$ -point. Table II display the band gap ( $E_g$ ) values simulated using both PBE and HSE06 functionals. We found that the  $E_g$  lies in the range 0.83 eV to 2.88 eV for different compounds. Clearly,  $E_g$  for NaCuSe (1.21 eV), KCuSe (1.28 eV), and KCuTe (1.62 eV) are most suitable for photovoltaic applications. It is also observed that the VBM at the  $\Gamma$ -point is doubly degenerate for crystal structures belonging to hexagonal symmetry *i.e.*,  $P6_3/mmc$  of ACu(S/Te) (Fig. 2(b,c,e,g)). A flat valence band edge is also observed in all the compounds, which can be very helpful for promising carrier transport due to their high effective masses.

Figure 3 shows the orbital projected partial density of states (PDOS) for all the ACuX compounds in the respective structures shown in Fig. 1. The PDOS reveals that the VBM mainly consists of the p- and d-orbitals of Cu and the p- orbital of S/Se/Te atoms at/near  $E_f$  for all the cases. The CBM is mainly contributed by the s-orbital of Na/K, p- and d-orbitals of Cu, and the s- and p-orbitals of S/Se/Te, respectively. It is also observed that the electronic states near  $E_f$  for alkali metals (Na or K) show a minimal contribution at VBM. The contributions of s-orbitals of alkali metals decrease near  $E_f$  as we move from ACuS to ACuSe and ACuTe. Unlike several

other chalcogenide based compounds, the  $E_g$  value in the present case first decreases as we go from Na/KCuS to Na/KCuSe, and then increases for Na/KCuTe. For example,  $E_g$  for NaCuS, NaCuSe and NaCuTe are 2.42 eV, 0.83 eV, and 1.21 eV respectively and a similar trend is obtained for KCuX systems as well. This is mainly attributed to the nature of hybridization between Cu and chalcogen atoms. The electronegativity values for different atoms are  $\chi_{Na} = 0.93$ ,  $\chi_K = 0.82$ ,  $\chi_{Cu} = 1.9$ , and  $\chi_{S/Se/Te} = 2.58/2.55/2.1$ , respectively. As chalcogen atoms are more electronegative than alkali metals, there is always an electronic charge transfer from the Na/K atom to S/Se/Te atoms. Similarly, the charge is also transformed from Cu atoms to S/Se atoms. However, a negligibly small charge transfer between Cu and Te atoms can be expected because their electronegativity is almost similar (the difference is 0.2). This is also reflected in their orbital PDOS plots. In order to better understand the role of hybridization in dictating the  $E_g$  trend, we show a zoomed-in view of the orbital projected PDOS above CBM for NaCuS, NaCuSe, and NaCuTe, respectively in Fig. S4(a,b,c) of SI[37]. A careful inspection of these plots clearly differentiate the orbital hybridization between Cu and S/Se/Te atoms at the CBM side. The electronic states of the p- and d- orbitals of Cu and the p orbitals of S atoms mainly contribute to the CBM side of NaCuS. Similarly, the CBM of NaCuSe consists of the s- and d-orbitals of Cu and the s-orbital of Se. However, the

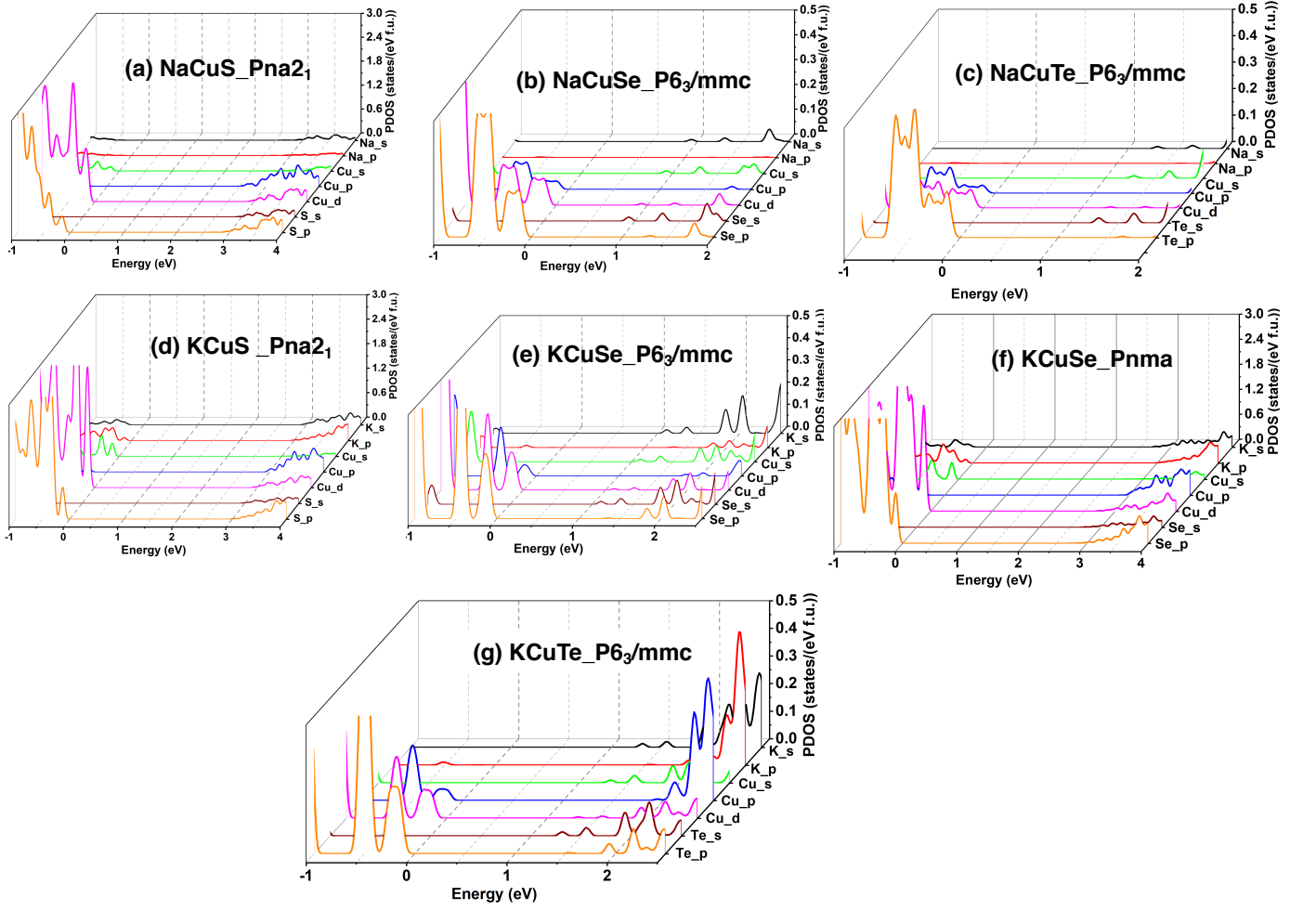


FIG. 3. Orbital projected partial density of states (PDOS) for ACuX (A=Na,K; X=S, Se, Te) compounds in the same respective structures as shown in Fig. 2.  $E_F$  is set at 0 eV.

nature of orbital hybridization in NaCuTe is quite different as compared to NaCuS and NaCuSe. Due to minimal charge transfer between Cu and Te, the orbital contributions from Cu-p, Cu-d, and Te-s are diminished near  $E_F$  and indicate only a strong hybridization between Na-s, Cu-s, and Te-p at the CBM side of NaCuTe, causing an increase in the band gap. Similar band gap trend and the orbital hybridization are also observed between Cu and Te atoms in KCuX compounds (see Fig. S4(d,e,f) of SI [37]) and can be explained on a similar ground. An analogous band gap trend is also observed in other chalcogenide based compounds like CdS, CdSe, and CdTe as well as ZnS, ZnSe, and ZnTe, respectively[38–40].

### C. Optical Properties

The band structure calculations established that all the ACuX compounds are direct band gap semiconductors, with the band gap falling in the range 0.83 eV to 2.88 eV. This motivates us to further study the optical

properties of these systems and evaluate their efficacy as solar absorber. Along with the absorption coefficient, we have calculated another screening parameter *i.e.*, spectroscopic limited maximum efficiency (SLME) proposed by Yu *et al.* [35]. SLME gives an upper bound on the solar efficiency by incorporating the nature/magnitude of band gap and absorption coefficient for a particular compound. It is an improvised version of the Shockley–Queisser (SQ) efficiency limit. Simulation of SLME also require the information about the possibility of optical transition from VBM to CBM for all the ACuX compounds. To obtain this, we have calculated the transition probability ( $p^2$ ) by calculating the square of transition dipole matrix elements. The transition probability for all the ACuX systems are shown in Fig. 2 (below each band structure plot). Clearly, direct optical transition from VBM to CBM is allowed for all the hexagonal structures of ACuSe/Te due to the finite  $p^2$  values at the high-symmetry point  $\Gamma$ . The optical transitions are allowed due to the same parity transition of electron states from p-states of S/Se/Te atoms at the VBM side to s–



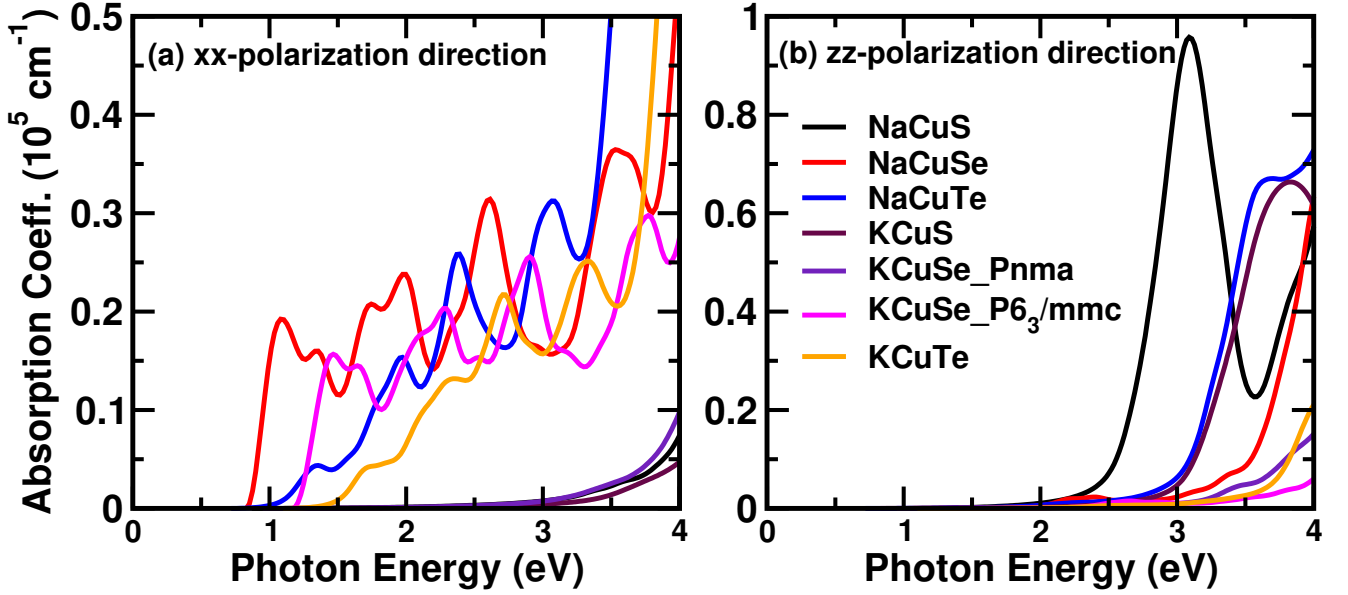


FIG. 4. Absorption coefficient ( $\alpha$ ) for ACuX (A=Na,K; X=S, Se, Te) along (a) x- and (b) z-polarization directions.

and p- states of Cu at the CBM side and d-states of Cu at VBM to s-states of S/Se/Te at CBM. In contrast, the  $p^2$  value is found to be zero at  $\Gamma$ -point for NaCuS, KCuS, and KCuSe (orthorhombic structures) in Fig. 2(a,d and f), indicating optically forbidden transition from VBM to CBM.

The absorption coefficient ( $\alpha$ ) of a given material is a quantifiable descriptor which dictate the penetration extent of a photon (with a particular wavelength) into the material before it gets absorbed. For a suitable solar absorber, a sharp rise in the absorption coefficient is obtained after the incidence of photon energy closer to its band gap.  $\alpha$  is related to the dielectric function and can be calculated using the following expression:

$$\alpha(E) = \frac{\sqrt{2}\omega}{c} \left[ \sqrt{\sqrt{\varepsilon_1^2(\omega) + \varepsilon_2^2(\omega)} - \varepsilon_1} \right] \quad (2)$$

where  $E$  is the incident photon energy,  $\omega$  is the angular frequency related to photon energy via  $E = \hbar\omega$  ( $\hbar$  is the reduced Planck's constant), and  $c$  is the speed of light in vacuum, respectively.  $\varepsilon_1$  and  $\varepsilon_2$  are the real and imaginary parts of the dielectric function. Figure 4(a,b) shows the absorption spectra plot for all ACuX compounds along the x- (left) and z-polarization (right) directions (arising out of structural anisotropy in hexagonal and orthorhombic structures). For orthorhombic systems (NaCuS, KCuS, KCuSe), the absorption spectra along the y-polarization direction are shown in Fig. S5 of SI[37]. The absorption onset for all the compounds is shifted to the band gap obtained from hybrid HSE06 calculations. Clearly, the absorption coefficients are not same along the three polarization directions because of the associated structural anisotropy. For example, in orthorhombic systems, the absorption coefficient of NaCuS

and KCuS is higher ( $\sim 0.6$  to  $0.9 \times 10^5 \text{ cm}^{-1}$ ) along the z-polarization direction than the x- and y-direction. However, the absorption coefficient of orthorhombic KCuS is high along y-polarization direction with respect to x- and z-direction (see Fig. S5). Similarly, for the hexagonal structures *i.e.*, KCuSe, KCuTe, NaCuSe, and NaCuTe, the simulated absorption coefficients fall in the range  $0.2 \times 10^5$  to  $0.6 \times 10^5 \text{ cm}^{-1}$  along x- and y-polarization directions, with a relatively small contribution arising from the z-direction as shown in Fig. 4(b).

Next, we have calculated the thickness dependence of SLME of all the ACuX compounds, considering the application for thin film solar cells. We have chosen four compounds *i.e.*, hexagonal ACu(Se/Te) (A=Na, K) because of their allowed optical transition and high absorption coefficients in the visible region. The thickness dependence of SLME is shown in Fig 5(a). Clearly, with increasing thickness, the SLME increases and then saturates beyond a certain thickness. The maximum SLME is found to be 18 % for a 10  $\mu\text{m}$  thick NaCuTe film. Similarly, for the rest of the ACuX systems, the SLME lie between  $\sim 10$  to 13%. Based on the optical and SLME descriptors, it is reasonable to consider that all the selenide and telluride based ACuX systems can be potential candidates for light absorbers in solar PV devices.

#### D. Potential Application in Photoelectrochemical (PEC) Water Splitting

We further investigate the feasibility of the ternary ACuX compounds for photocatalytic water splitting applications. We calculated the band edge positions with respect to the water redox levels[41, 42] using the empirical model proposed by Butler and Ginley[43]. According

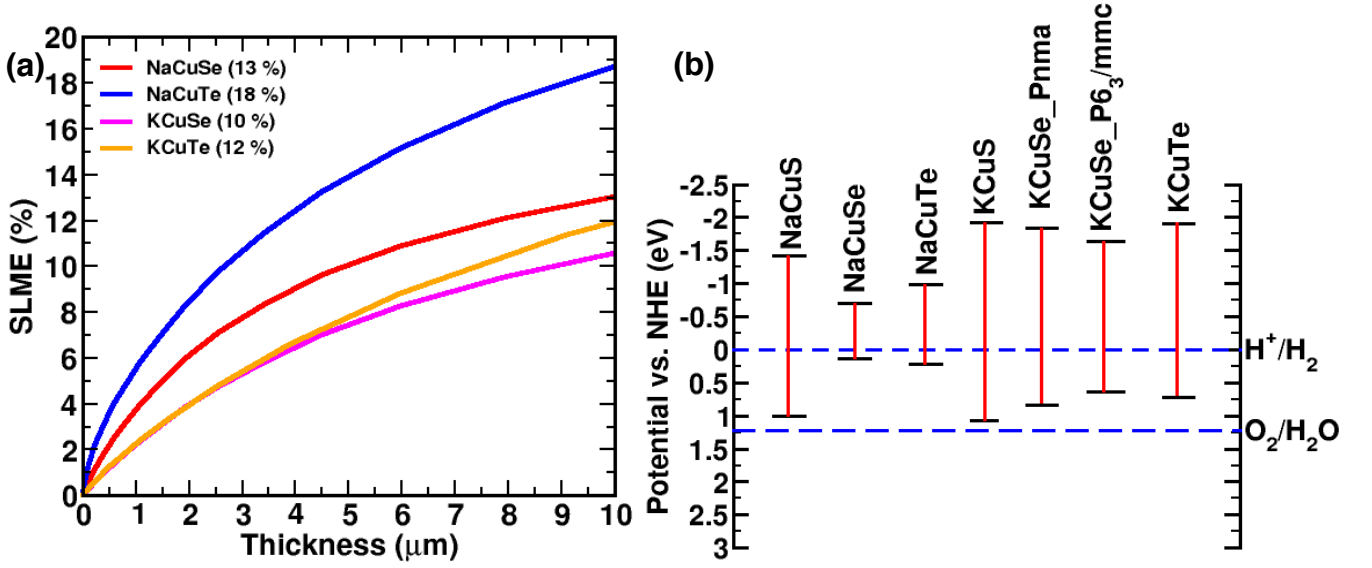


FIG. 5. (a) Spectroscopic Limited Maximum Efficiency, SLME (at 300 K) vs. film thickness for the hexagonal ACuX compounds whose band gaps lie in the visible region. (b) Band edge positions with respect to water redox levels for all stable ACuX compounds.

to their model, the valence and conduction band edge positions can be obtained from the following expression,

$$E_{VBE/CBE} = E_0 + (\chi_A \chi_{Cu} \chi_X)^{1/3} \pm \frac{E_g}{2} \quad (3)$$

where  $E_0$  is the difference between a normal hydrogen electrode (NHE) and vacuum whose value is -4.5 eV.  $\chi$  is the electronegativities of the constituent elements in the Mulliken scale, and  $E_g$  is the band gap. Figure 5(b) shows the band edge positions for all the stable ACuX compounds. For a compound to be promising for PEC water splitting, the CBM must locate more negative than the redox potential of H<sup>+</sup>/H<sub>2</sub> (0 V *vs.* NHE), and the VBM must align more positive than the redox potential of O<sub>2</sub>/H<sub>2</sub>O (1.23 V *vs.* NHE) at ambient condition[44]. As evident from Fig. 5(b), it is clear that all ternary copper chalcogenides have a well positioned conduction band edge to be used as photocathode for hydrogen evolution reaction (HER) in a PEC cell.

#### IV. CONCLUSION

In conclusion, we have systematically investigated the chemical/dynamical stability and optoelectronic properties of ternary ACuX (A=Na, K; X=S, Se, Te) chalcogenides using first-principles calculations. The structural stability metrics ensure that NaCuS, KCuS and KCuSe crystallize in orthorhombic structure while NaCuSe/Te and KCuTe stabilize in hexagonal phase. Interestingly, few of these compounds show intriguing energetics/phonon trends, which suggests them to stabilize in structure(s) other than that predicted experimentally

(one report only). This demands for a revisit of the crystal structure prediction. All the compounds are direct band gap semiconductors having band gaps laying between 0.83 eV to 2.88 eV. The direct optical transitions are forbidden for orthorhombic systems (NaCuS, KCuS, and KCuSe), while it is allowed for the remaining systems (hexagonal phase). The absorption coefficient for the optically allowed ACuX compounds lie in the range  $\sim (0.2 \text{ to } 0.6) \times 10^5 \text{ cm}^{-1}$  in the visible region. The highest simulated efficiency for the NaCuTe is determined to be 18% for an 8 μm thick film. In addition, the favorable straddling of valence band edges with respect to the normal hydrogen electrodes confirms the suitability of all these compounds as photocathodes for the hydrogen evolution reaction (HER) in the photoelectrochemical (PEC) process. The present study suggests that the ternary alkali metal-based copper chalcogenides can be suitable candidates as light absorbers in PV cells as well as photocathodes for HER in photocatalytic water splitting applications, requiring further experimental investigation.

#### ACKNOWLEDGEMENTS

G.B. would like to thank the Council of Scientific and Industrial Research (CSIR), India, for providing senior research fellowship. N.S. acknowledge the financial support from the Khalifa University of Science and Technology under the Emerging Science & Innovation Grant ESIG-2023-004 and the contribution of Khalifa University's high-performance computing and research computing facilities to the results of this research.



- [1] B. Saparov, Next generation thin-film solar absorbers based on chalcogenides, *Chem. Rev.* **122**, 10575 (2022).
- [2] S. Palchoudhury, K. Ramasamy, and A. Gupta, Multinary copper-based chalcogenide nanocrystal systems from the perspective of device applications, *Nanoscale Adv.* **2**, 3069 (2020).
- [3] D. Shin, B. Saparov, and D. B. Mitzi, Defect engineering in multinary earth-abundant chalcogenide photovoltaic materials, *Adv. Energy Mater.* **7**, 1602366 (2017).
- [4] I. Sharma, P. S. Pawar, R. K. Yadav, R. Nandi, and J. Heo, Review on bandgap engineering in metal-chalcogenide absorber layer via grading: a trend in thin-film solar cells, *Sol Energy*. **246**, 152 (2022).
- [5] A. Polman, M. Knight, E. C. Garnett, B. Ehrler, and W. C. Sinke, Photovoltaic materials: Present efficiencies and future challenges, *Science* **352**, aad4424 (2016).
- [6] A. G. Martin, E. Keith, H. Yoshihiro, and W. Wilhelm, Solar cell efficiency tables (version 33), *Prog. Photovoltaics: Res. Appl.* **17**, 85 (2008).
- [7] S. Ouendadji, S. Ghemid, H. Meradji, and F. E. H. Hassan, Theoretical study of structural, electronic, and thermal properties of CdS, CdSe and CdTe compounds, *Comput. Mater. Sci.* **50**, 1460 (2011).
- [8] S. Eyderman, A. Deinega, and S. John, Near perfect solar absorption in ultra-thin-film GaAs photonic crystals, *J. Mater. Chem. A* **2**, 761 (2014).
- [9] S. D. Stranks, G. E. Eperon, G. Grancini, C. Menelaou, M. J. Alcocer, T. Leijtens, L. M. Herz, A. Petrozza, and H. J. Snaith, Electron-hole diffusion lengths exceeding 1 micrometer in an organometal trihalide perovskite absorber, *Science* **342**, 341 (2013).
- [10] X. Liu, K. Matsuda, Y. Moritomo, A. Nakamura, and N. Kojima, Electronic structure of the gold complexes  $\text{Cs}_2\text{Au}_2\text{X}_6$  (X= I, Br, and Cl), *Phys. Rev. B* **59**, 7925 (1999).
- [11] W. E. Sha, X. Ren, L. Chen, and W. C. Choy, The efficiency limit of  $\text{CH}_3\text{NH}_3\text{PbI}_3$  perovskite solar cells, *Appl. Phys. Lett.* **106**, 221104 (2015).
- [12] S. D. Stranks, V. M. Burlakov, T. Leijtens, J. M. Ball, A. Goriely, and H. J. Snaith, Recombination kinetics in organic-inorganic perovskites: excitons, free charge, and subgap states, *Phys. Rev. Appl.* **2**, 034007 (2014).
- [13] W. Tress, J. P. Correa Baena, M. Saliba, A. Abate, and M. Graetzel, Inverted current-voltage hysteresis in mixed perovskite solar cells: polarization, energy barriers, and defect recombination, *Adv. Energy Mater.* **6**, 1600396 (2016).
- [14] D. Dahliah, G. Brunin, J. George, V.-A. Ha, G.-M. Rignanes, and G. Hautier, High-throughput computational search for high carrier lifetime, defect-tolerant solar absorbers, *Energy Environ. Sci.* **14**, 5057 (2021).
- [15] G. Savelsberg, Ternäre Pnictide und Chalkogenide von Alkalimetallen und IB-bzw. IIB-Elementen/On ternary pnictides and chalcogenides of alkaline metals and IB-resp. II B-elements, *Zeitschrift für Naturforschung B* **33**, 370 (1978).
- [16] G. Savelsberg and H. Schäfer, Darstellung und Kristallstruktur von  $\text{Na}_2\text{AgAs}$  und  $\text{KCuS}$ /Preparation and Crystal Structure of  $\text{Na}_2\text{AgAs}$  and  $\text{KCuS}$ , *Zeitschrift für Naturforschung B* **33**, 711 (1978).
- [17] A. Parveen and G. Vaitheeswaran, Exploring exemplary optoelectronic and charge transport properties of  $\text{KCuX}$  (X= Se, Te), *Sci. Rep.* **8**, 1 (2018).
- [18] M. Boualleg, B. Bennecer, and F. Kalarasse, Ab initio predictions of structures and physical properties of the  $\text{KCuX}$  (X= Se and Te) phases under pressure, *Comput. Condens. Matter* **30**, e00616 (2022).
- [19] A. R. Oganov, A. O. Lyakhov, and M. Valle, How Evolutionary Crystal Structure Prediction Works- and Why, *Acc. Chem. Res.* **44**, 227 (2011).
- [20] A. O. Lyakhov, A. R. Oganov, H. T. Stokes, and Q. Zhu, New developments in evolutionary structure prediction algorithm USPEX, *Comput. Phys. Commun.* **184**, 1172 (2013).
- [21] A. R. Oganov and C. W. Glass, Crystal structure prediction using ab initio evolutionary techniques: Principles and applications, *J. Chem. Phys.* **124** (2006).
- [22] J. P. Perdew, K. Burke, and M. Ernzerhof, Generalized gradient approximation made simple, *Phys. Rev. Lett.* **78**, 1396 (1997).
- [23] J. P. Perdew, K. Burke, and M. Ernzerhof, Generalized gradient approximation made simple, *Phys. Rev. Lett.* **77**, 3865 (1996).
- [24] G. Kresse and J. Furthmüller, Efficiency of ab-initio total energy calculations for metals and semiconductors using a plane-wave basis set, *Comput. Mater. Sci.* **6**, 15 (1996).
- [25] G. Kresse and J. Hafner, Ab initio molecular dynamics for liquid metals, *Phys. Rev. B* **47**, 558 (1993).
- [26] G. Kresse and J. Furthmüller, Efficient iterative schemes for ab initio total-energy calculations using a plane-wave basis set, *Phys. Rev. B* **54**, 11169 (1996).
- [27] J. Heyd, G. E. Scuseria, and M. Ernzerhof, Hybrid functionals based on a screened coulomb potential, *J. Chem. Phys.* **118**, 8207 (2003).
- [28] J. Heyd and G. E. Scuseria, Efficient hybrid density functional calculations in solids: Assessment of the heyd-scuseria-ernzerhof screened coulomb hybrid functional, *J. Chem. Phys.* **121**, 1187 (2004).
- [29] P. E. Blöchl, O. Jepsen, and O. K. Andersen, Improved tetrahedron method for Brillouin-zone integrations, *Phys. Rev. B* **49**, 16223 (1994).
- [30] A. Togo and I. Tanaka, First principles phonon calculations in materials science, *Scr. Mater.* **108**, 1 (2015).
- [31] K. Parlinski, Z. Li, and Y. Kawazoe, First-principles determination of the soft mode in cubic  $\text{ZrO}_2$ , *Phys. Rev. Lett.* **78**, 4063 (1997).
- [32] M. Gajdoš, K. Hummer, G. Kresse, J. Furthmüller, and F. Bechstedt, Linear optical properties in the projector-augmented wave methodology, *Phys. Rev. B* **73**, 045112 (2006).
- [33] S. L. Adler, Quantum theory of the dielectric constant in real solids, *Phys. Rev.* **126**, 413 (1962).
- [34] N. Wiser, Dielectric constant with local field effects included, *Phys. Rev.* **129**, 62 (1963).
- [35] L. Yu and A. Zunger, Identification of potential photovoltaic absorbers based on first-principles spectroscopic screening of materials, *Phys. Rev. Lett.* **108**, 068701 (2012).
- [36] M. Bercx, R. Saniz, B. Partoens, and D. Lamoen, Exceeding the shockley-queisser limit within the detailed balance framework, Many-body Approaches at Different

- Scales: A Tribute to Norman H. March on the Occasion of his 90th Birthday , 177 (2018).
- [37] See Supporting Information at [URL] for further theoretical backgrounds, the formation energies in for different space group lattices of ACuX compound and their phonon dispersion plots for the energetically most stable structures, SOC band structures and absorption spectra of orthorhombic structures along  $yy$ -polarization direction.
  - [38] E. Deligoz, K. Colakoglu, and Y. Ciftci, Elastic, electronic, and lattice dynamical properties of cds, cdse, and cdte, *Phys. B: Condens. Matter* **373**, 124 (2006).
  - [39] Y. Duan and M. Jungen, Electronic structural and magnetic properties of cadmium chalcogenide beryllosilicate sodalites, *Eur. Phys. J. B* **2**, 183 (1998).
  - [40] O. Zakharov, A. Rubio, X. Blase, M. L. Cohen, and S. G. Louie, Quasiparticle band structures of six ii-vi compounds: Zns, znse, znse, cds, cdse, and cdte, *Phys. Rev. B* **50**, 10780 (1994).
  - [41] Y. Xu and M. A. Schoonen, The absolute energy positions of conduction and valence bands of selected semiconducting minerals, *Am. Min* **85**, 543 (2000).
  - [42] I. E. Castelli, F. Hüser, M. Pandey, H. Li, K. S. Thygesen, B. Seger, A. Jain, K. A. Persson, G. Ceder, and K. W. Jacobsen, New light-harvesting materials using accurate and efficient bandgap calculations, *Adv. Energy Mater.* **5**, 1400915 (2015).
  - [43] M. Butler and D. Ginley, Prediction of flatband potentials at semiconductor-electrolyte interfaces from atomic electronegativities, *J. Electrochem. Soc.* **125**, 228 (1978).
  - [44] V. Chakrapani, J. C. Angus, A. B. Anderson, S. D. Wolter, B. R. Stoner, and G. U. Sumanasekera, Charge transfer equilibria between diamond and an aqueous oxygen electrochemical redox couple, *Science* **318**, 1424 (2007).